ACS APPLIED MATERIALS & INTERFACES

Research Article

www.acsami.org

Highly Transparent Carbon Counter Electrode Prepared via an in Situ Carbonization Method for Bifacial Dye-Sensitized Solar Cells

Chenghao Bu, Yumin Liu, Zhenhua Yu, Sujian You, Niu Huang, Liangliang Liang, and Xing-Zhong Zhao*

School of Physics and Technology, Key Laboratory of Artificial Micro/Nano Structures of Ministry of Education, Wuhan University, Wuhan 430072, China

Supporting Information

ABSTRACT: A facile in situ carbonization method was demonstrated to prepare the highly transparent carbon counter electrode (CE) with good mechanical stability for bifacial dye-sensitized solar cells (DSCs). The optical and electrochemical properties of carbon CEs were dramatically affected by the composition and concentration of the precursor. The well-optimized carbon CE exhibited high transparency and sufficient catalytic activity for I_3^- reduction. The bifacial DSC with obtained carbon CE achieved a high power conversion efficiency (PCE) of 5.04% under rear-side illumination, which approaches 85% that of front-side illumination (6.07%). Moreover, the device shows excellent stability as confirmed by the aging test. These promising results reveal the enormous potential of this transparent carbon CE in scaling up and commercialization of low cost and effective bifacial DSCs.

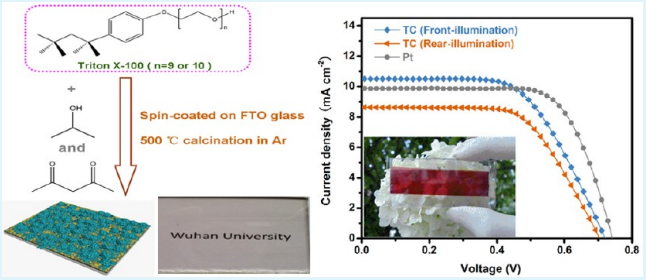

KEYWORDS: *in situ carbonization method, transparent carbon counter electrode, optical and electrochemical properties, bifacial dye-sensitized solar cells, long-term stability*

1. INTRODUCTION

On the basis of the operation principle similar to natural photosynthesis, dye-sensitized solar cells (DSCs) have been proposed as reliable alternatives to conventional silicon solar cells.[1−3] Although the DSCs possess many advantages such as environmental-friendliness, easy fabrication, and considerable power conversion efficiency (PCE),[4,5] the relative high cost of core materials[6] and finite utilization of sunlight still restrict their commercial application. Therefore, further reduction of cost and the more practical system of DSCs are common concerns for their development.

The traditional platinum counter electrode (CE), which exhibits high catalytic activity for reducing the I_3^- to I^- by electron migrating through the external circuit and completing the regenerative cycle, is considered to be unsuitable for mass production of DSCs due to its drawbacks of scarce resource and high expense.[7,8] Hence, seeking other cheaper materials to replace platinum as electrochemical catalysts on CEs is an approach to further bring down the final costs of devices. Among all the alternative catalysts to platinum,[7,8] carbonaceous materials including graphite,[9] carbon black,[10] carbon nanofiber,[11] carbon nanotube,[12−14] well-ordered mesoporous carbon,[15] and graphene[16,17] have attracted extensive attention due to their low cost, nontoxicity, and reasonable catalytic activity. Despite the advantages mentioned above, there still remains two unsolved problems for carbon CEs. One is the poor connection between carbon film and substrate, which restrains the long-term use of the carbon CEs.[8] The other is that thick film (about several tens of micrometers) is required for conventional carbon CEs to attain desired catalytic activity, which limits their optical transmittance and leads to difficulty in fabricating bifacial DSCs.[18] The concept of bifacial DSCs was proposed by J. Bisquert in 2008, and Ito et al. have reported the semitransparent Pt CE-based bifacial DSC with a PCE of 5.96% under rear-illumination.[19,20] In recent years, some bifacial DSCs based on conducting polymer CEs have also been described.[18,21,22] Compared to the traditional DSCs that can only work under the front-illumination, bifacial DSCs are able to convert incident sunlight to electricity from both sides of the devices, leading to enhanced light harvest. Therefore, it is essential to develop bifacial DSCs based on transparent carbon CEs to further bring down the production cost.[8,19,20] Though the optically transparent CE based on graphene nanoplatelets have been reported by L. Kavan et al. in 2011,[23] the relative high cost and the complicated preparation process of graphene stimulate us to explore a more economical and facile method for fabricating the transparent carbon CE, which can meet all the requirements involving sufficient electrochemical catalytic activity, high transparency, and good mechanical stability.

Herein, for the first time, we report a highly transparent carbon CE prepared by a facile in situ carbonization method and its application in bifacial DSCs. The CE was fabricated by

Received: May 9, 2013
Accepted: June 28, 2013
Published: June 28, 2013

   dx.doi.org/10.1021/am4017472 | ACS Appl. Mater. Interfaces 2013, 5, 7432−7438

Scheme 1. Illustration of the Preparation Process and the Nanostructure of Different Transparent Carbon Counter Electrodes

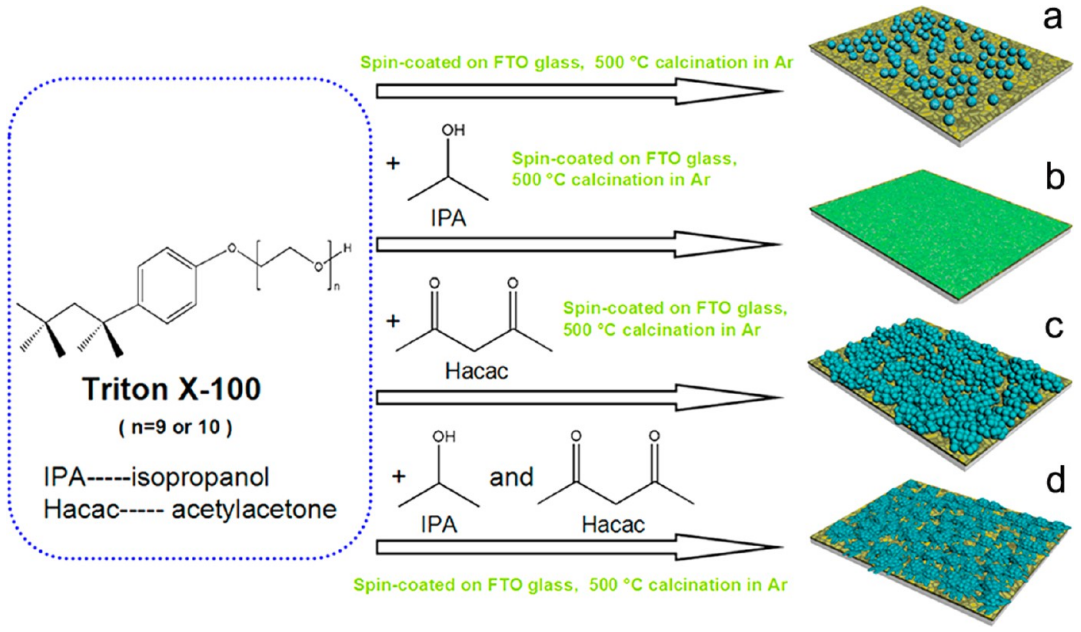

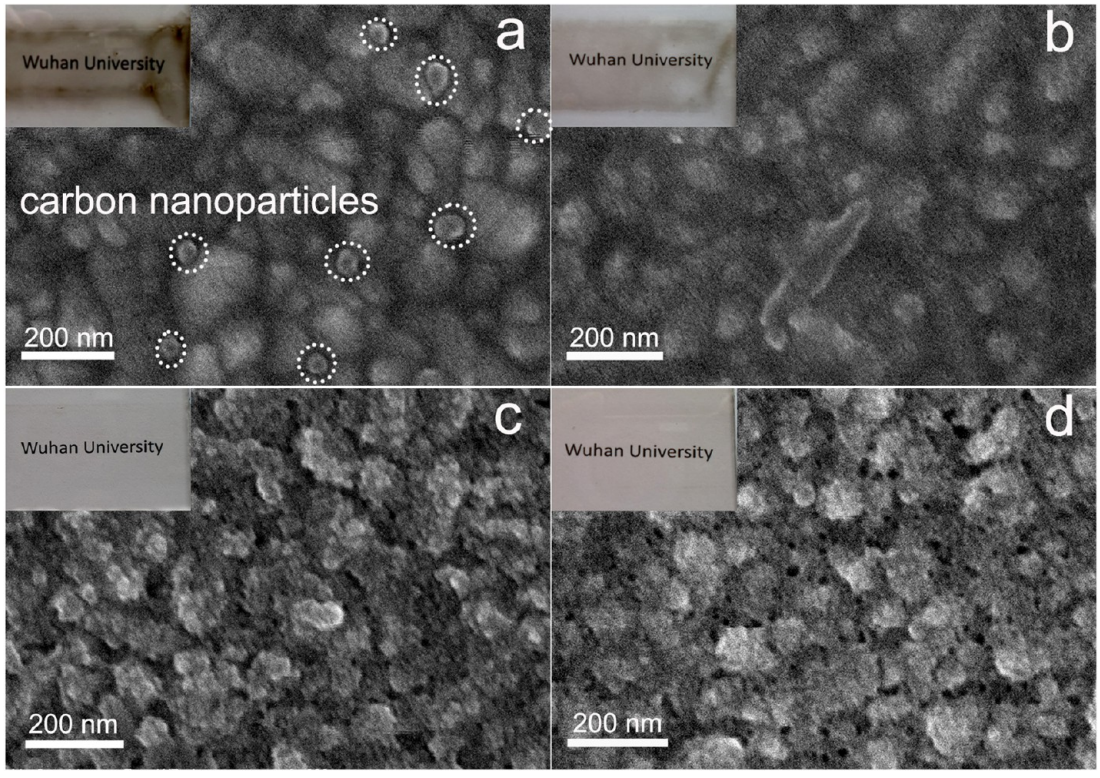

Figure 1. SEM images and digital photographs (the insets) of the transparent carbon counter electrodes prepared by the precursor consist of (a) pure Triton X-100, (b) isopropanol + Triton X-100, (c) acetylacetone + Triton X-100, and (d) isopropanol + acetylacetone + Triton X-100.

coating FTO glass with mixed solution and directly sintering at 500 °C in argon atmosphere. Through adjusting the composition of precursor, the micromorphology and electrocatalytic activity of carbon CEs have been optimized. In comparison with conventional carbon CEs, the CE prepared by this method achieved excellent mechanical stability, as confirmed by the long-term stability test. More importantly, high optical transmittance demonstrated by UV−vis transmitted spectra make the carbon CE suitable for being applied in bifacial DSCs. On the basis of the optimized conditions, the device showed PCE of 6.07% and 5.04% corresponding to front- and rear-side illumination, respectively. To our knowledge, this result shows the highest PCE ratio (PCE_R/PCE_F) between the two operating modes in Pt-free bifacial DSCs (the PCE_R/PCE_F was generally about 50−70% according to the previous reports[18,21,22]). Our work paves a way to develop new carbon CEs that can simultaneously overcome the disadvantages of opaque and poor mechanical stability; the influence of

dx.doi.org/10.1021/am4017472 | ACS Appl. Mater. Interfaces 2013, 5, 7432−7438

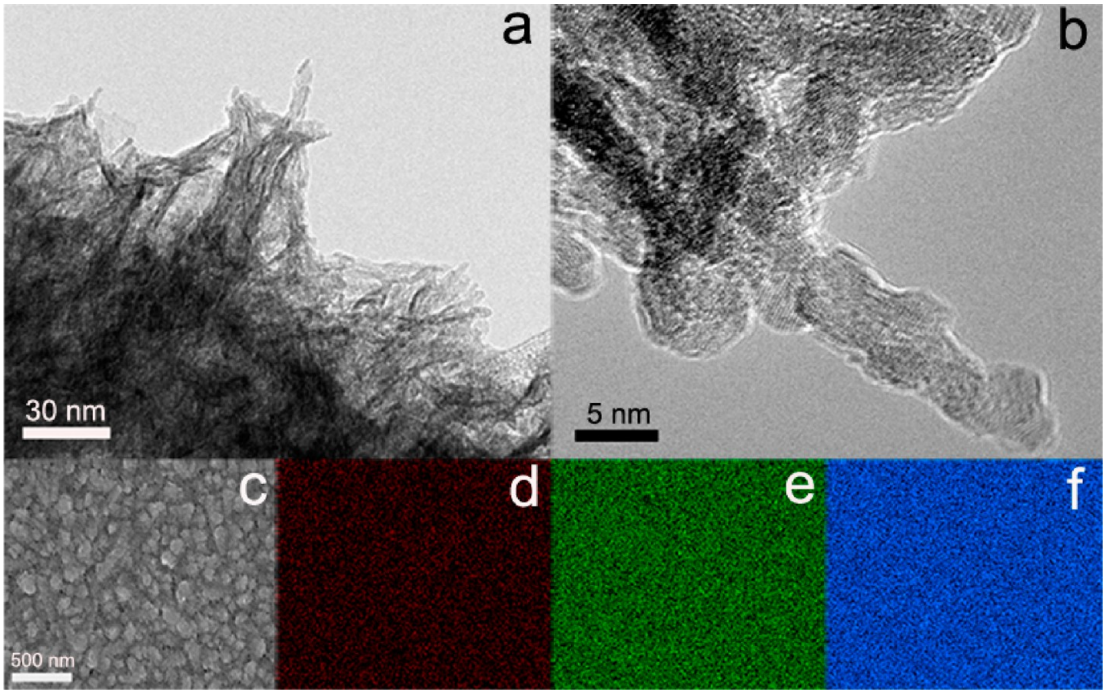

Figure 2. (a, b) TEM and HRTEM of carbon film exfoliated from the CE IPA/Hacac/TX-100, (c) a low magnification SEM image of CE IPA/Hacac/TX-100, and EDX mapping of (d) carbon, (e) oxygen, and (f) tin elements.

different precursors on the optical and electrochemical properties of these new carbon CEs are the focus of attention in this paper.

2. RESULT AND DISCUSSION

Scheme 1 schematically depicts the preparation process and nanostructure of different transparent carbon CEs. Their micromorphologies are affected by the precursor, as characterized by scanning electron microscopy (SEM) and shown in Figure 1. The carbonized film prepared by pure Triton X-100 would shrink and become single scattered carbon nanoparticles on FTO glass (as pointed out by the dashed boxes in Figure 1a). By adding isopropanol to the precursor, the carbon nanoparticles aggregated and formed a compact coating layer (Figure 1b). When isopropanol was replaced by acetylacetone, Triton X-100 could uniformly disperse in the precursor, leading to a rough film consisting of stacked spheres (Figure 1c). Furthermore, the incontinuous stacked carbon spheres would connect with each other by tentacles, and the film exhibited net-like structure (Figure 1d) if the ternary solution (isopropanol + acetylacetone + Triton X-100) was used as the precursor. It is noteworthy that carbon film was not obtained if the precursor contained only isopropanol or acetylacetone and the CE exhibited the same morphology of pure FTO as shown in Figure S1 in the Supporting Information. This phenomenon could be attributed to the low boiling points of isopropanol and acetylacetone, which make them easy to be evaporated before carbonization.

It could be suggested that the Triton X-100 is a requisite and acts as carbon source in our experiment, while the isopropanol and acetylacetone are regarded as solvent and dispersant, which play an important role in nanostructure formation of final carbonized film. For simplicity, the carbon CEs prepared by pure Triton X-100, isopropanol + Triton X-100, acetylacetone + Triton X-100, and isopropanol + acetylacetone + Triton X-100 are labeled as CE TX-100, CE IPA/TX-100, CE Hacac/TX-100, and CE IPA/Hacac/TX-100, respectively, in the following narration. The digital photos of different carbon CEs are shown in the inset of Figure 1. They all display high transparency except the CE TX-100.

Figure 2c–f presents the SEM energy-dispersive X-ray (SEM-EDX) images of CE IPA/Hacac/TX-100. The uniform distribution of the C, O, and Sn atoms have been revealed, which confirms that homogeneous carbon film have been successfully prepared on FTO glass. The detailed structural characterization by TEM (Figure 2a,b) shows that the porous carbon film is composed of intercrossed nanosheets, which connect with each other and form a branch-like structure. We deduce that the special structure can generate abundant defective sites and sufficient surface area to achieve desired catalytic activity for the reduction of I_3^-.[24,10]

Figure 3a shows the optical transmitted spectra of as-prepared four carbon CEs. By using the pure FTO glass as the reference, CE IPA/TX-100, CE Hacac/TX-100, and CE IPA/Hacac/TX-100 all present excellent transparency ranging from 400 to 800 nm, which is desirable and beneficial for the rear-side illumination of bifacial DSCs due to the complementary absorption properties between these new carbon CEs and N3 dye (the absorption of N3 dye is mainly in the range of 450–600 nm).[18] The transmittance of CE TX-100 is relatively low but still more than 30% of that achieved by FTO glass. These results reveal that the in situ carbonization method is feasible for fabricating transparent carbon CEs. Raman spectra of CE TX-100, CE IPA/TX-100, CE Hacac/TX-100, and CE IPA/Hacac/TX-100 are presented in Figure 3b. The two characteristic bands (the D band at 1365 cm^{-1} and the G band at 1590 cm^{-1}, attributed to disordered carbonaceous component and ordered graphitic component, respectively)[25] are observed for all the CEs, which could further confirm that the carbon catalysts have been successfully prepared on FTO glass by four different precursors. (The two characteristic bands are not found for the FTO glass.) The intensity ratio of D-peak to G-

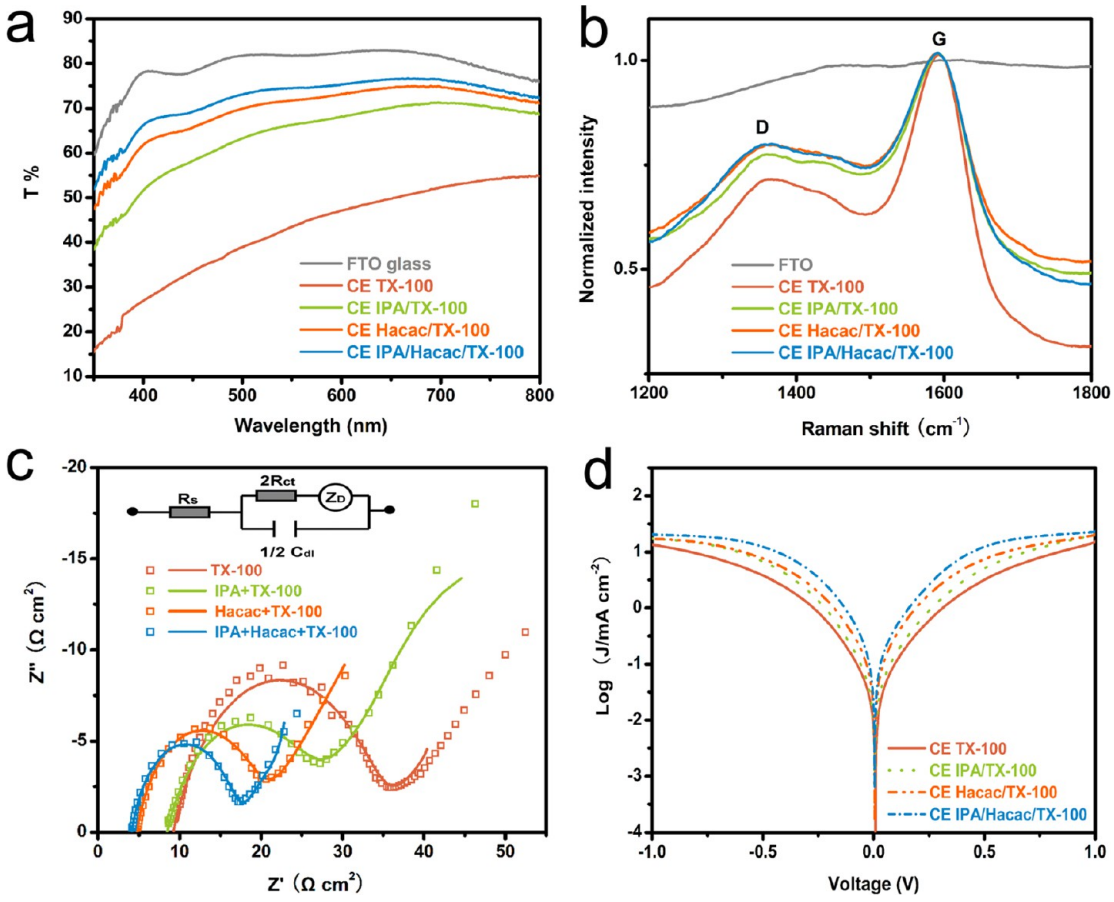

Figure 3. (a) UV−vis transmitted spectra of FTO glass and transparent carbon counter electrodes prepared by different precursors. (b) Raman spectra of the transparent carbon counter electrodes prepared by different precursors; the Raman intensities are normalized to the corresponding G-band intensities. (c) Nyquist plots of the symmetrical cells fabricated with the transparent carbon counter electrodes prepared by different precursors; the symbols are experimental data, and the solid lines are fitted results according to the inset equivalent circuit. (d) Tafel curves of the different symmetrical cells that are the same as the ones used in EIS measurements.

peak (I_D/I_G) is introduced to investigate the defects and structure disorder of four carbon CEs, and the data are shown in Table S1 (in the Supporting Information). The CE IPA/Hacac/TX-100 exhibits higher I_D/I_G (0.786) than that of other CEs, indicating a large number of defects and open edges on it,[26] which will enhance the electrocatalytic activity of this CE. This result confirms our deduction in the discussion of TEM images.

In order to examine the electrochemical characteristics of the four carbon CEs, electrochemical impedance spectroscopy (EIS) experiments and Tafel polarization measurements were carried out with symmetrical cells. The symmetrical cells were made by assembling two identical electrodes on each side separated by a spacer containing an electrolyte used in full function DSCs.[27] Figure 3c shows the typical Nyquist plots of the symmetrical cells based on four different carbon electrodes. According to the equivalent circuit in the inset, the intersection of high frequency semicircle at real axis represents the series resistance (R_s). The diameter of high frequency semicircle represents the charge transfer resistance (R_{ct}) at the CE/electrolyte interface. The low frequency arc arises from the Nernst diffusion impedance of the redox couple in electrolyte.[28] The R_s and R_{ct} for all CEs were fitted, and the results are listed in Table S1 (in the Supporting Information). Since the R_{ct} varies inversely with the electrocatalytic activity for the reduction of I_3^-, the lower R_{ct} of the CE IPA/Hacac/TX-100 (12.5 Ω cm^2) than that of CE TX-100 (25.38 Ω cm^2), CE IPA/TX-100 (18.13 Ω cm^2), and CE Hacac/TX-100 (15 Ω cm^2) illustrates that the CE IPA/Hacac/TX-100 has the best catalytic activity for I_3^- reduction among the four CEs. In addition, the CE IPA/Hacac/TX-100 has the smallest R_s values (4.14 Ω cm^2), which reveals its highest conductivity and will contribute to the improvement of cell performance.[29] The Tafel curves of the four CEs are shown in Figure 3d. In the tafel zone, the anodic and cathodic branches of the curves display a larger slope for the CE IPA/Hacac/TX-100 compared to the other three CEs, indicating a larger exchange current density (J_0) on the surface of this electrode. The relationship between the J_0 and the R_{ct} extracted from EIS follows the equation below:

$$J_0 = \frac{RT}{nFR_{ct}}$$

where the R, T, F, and n are the gas constant, the temperature, the Faraday's constant, and the number of electrons involved in the reduction of I_3^-.[29,30] Hence, the larger J_0 means the lower R_{ct} and higher electrocatalytic activity of the CE IPA/Hacac/TX-100. This result is in good agreement with the EIS measurement. The relative high electrocatalytic activity of the CE IPA/Hacac/TX-100 is ascribed to its abundant defects and considerable surface area as exhibited by SEM, TEM, and Raman spectra.

dx.doi.org/10.1021/am4017472 | ACS Appl. Mater. Interfaces 2013, 5, 7432−7438

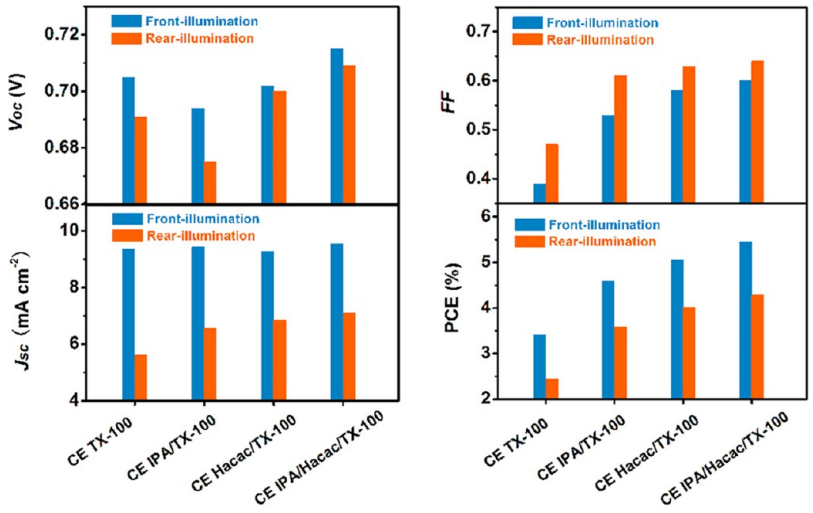

Figure 4. The influences of different carbon counter electrodes on photovoltaic parameters of bifacial DSCs. The data were measured under AM 1.5 simulated irradiation (75 mW cm^{-2}) with an active area of 0.24 cm^2.

To understand the effect of different carbon CEs on the cell performance, the photocurrent density−voltage (J−V) curves of bifacial DSCs employing CE TX-100, CE IPA/TX-100, CE Hacac/TX-100, and CE IPA/Hacac/TX-100 measured under AM 1.5 simulated sunlight (75 mW cm^{-2}) are shown in Figure S2 (in the Supporting Information). The resultant photovoltaic parameters and their variations are summarized in Table S2 (in the Supporting Information) and Figure 4, respectively. In the case of front-illumination, the open-circuit voltage (V_{oc}) and the short-circuit photocurrent density (J_{sc}) presents the irregular variations with different CEs. However, the fill factor (FF) increases dramatically from 0.39 to 0.60 in the order of CE TX-100 (0.39), CE IPA/TX-100 (0.53), CE Hacac/TX-100 (0.58), and CE IPA/Hacac/TX-100 (0.60), which is attributed to the increasing electrocatalytic activity of the four CEs in the same order depicted in EIS and Tafel polarization measurement. As a result, the power conversion efficiency (PCE) monotonically increased from 3.4% (CE TX-100) to 5.45% (CE IPA/Hacac/TX-100). In the case of rear-illumination, less incident light can be absorbed by N3 dye due to the absorption of the carbon CE and the I_3^- in the electrolyte, leading to lower J_{sc} compared to the front-illumination conditions. The improvement of FF and the reduction of V_{oc} are attributed to the same reason; the detailed explanation of the relationship between the photovoltaic parameters and light intensity has been given in the literature.[31,32] In the order of CE TX-100, CE IPA/TX-100, CE Hacac/TX-100, and CE IPA/Hacac/TX-100, the V_{oc} still shows the irregular variations, but the J_{sc}, the FF, and the PCE all increase monotonically. We attribute the increasing J_{sc} to the higher light harvest of dye caused by the enhanced optical transmittance of CEs (CE IPA/Hacac/TX-100 > CE Hacac/TX-100 > CE IPA/TX-100 > CE TX-100, as shown in Figure 3a).

Thus, the CE IPA/Hacac/TX-100 can be recommended as the optimal CE, which will be used for the further investigation. The influence of CEs derived from precursor with different TX-100 concentration (the volume ratio of TX-100 to [IPA+ Hacac] was used as the parameter) on the cell performance was also investigated, and the detailed photovoltaic parameters are listed in Table S3 (in the Supporting Information). As demonstrated in Figure S3a (in the Supporting Information), in both cases (front and rear-illumination), the PCE of devices first increases with the increasing volume ratio of TX-100 to (IPA+ Hacac). The highest values of 5.58% (front-illumination) and 4.10% (rear-illumination) were achieved when the volume ratio of TX-100 to (IPA+ Hacac) is 0.50, then it decreases with a further increase in the volume ratio. In the case of front-illumination, the increasing PCE is mainly ascribed to the increasing electrocatalytic activity of the carbon CEs before the volume ratio reaches 0.5. However, when the volume ratio exceeds 0.5, the CEs exhibit the similar appearance (see Figure S3b in the Supporting Information) and electrocatalytic activity to the CE TX-100, which lead to the deterioration of cell performance. On the other hand, in the case of rear-illumination, when the CE derived from precursor with low TX-100 concentration was used, the positive effect of improved optical transparency (shown in Figure S3b in the Supporting Information) on the PCE was offset by the decreased electrocatalytic activity. As a result, the PCE still increases monotonically until the volume ratio reaches 0.5. Hence, the properties of transparent carbon CE have been optimized by using the ternary precursor (IPA + Hacac + TX-100) with the volume ratio $[V_{TX\text{-}100}/V_{(IPA+Hacac)}]$ of 0.5.

By further optimizing the TiO_2 photoanodes and the N3 dye, we present the J−V curves measured under AM 1.5 simulated irradiation at 75 mW cm^{-2} for our best performing bifacial DSC in Figure 5a. The resultant photovoltaic parameters are given in Table 1. The device gives a V_{oc} of 721 mV, a J_{sc} of 10.54 mA cm^{-2}, and a FF of 0.60, leading to a PCE as high as 6.07% under front-side illumination, which approaches 90% that of the device with the Pt CE (6.89%). It is unexpected that the J_{sc} of the device based on transparent carbon CE is even slightly higher than that of Pt CE. We deduce that this phenomenon is attributed to the porous and rough surface structure of transparent carbon CE as presented by SEM and TEM. The reduced FF is the main reason for the efficiency loss, which suggests that the catalytic activity of the transparent carbon CE is still inferior to the Pt CE (the electrochemical characterizations of Pt CE are shown in Figure S4 in the Supporting Information), and the effort to further enhance the catalytic activity of this carbon CE will be made in the future work. It is surprising that the PCE of 5.04% under rear-side illumination is achieved for our best performing device. The high PCE of the bifacial DSC under rear-side illumination can be ascribed to the

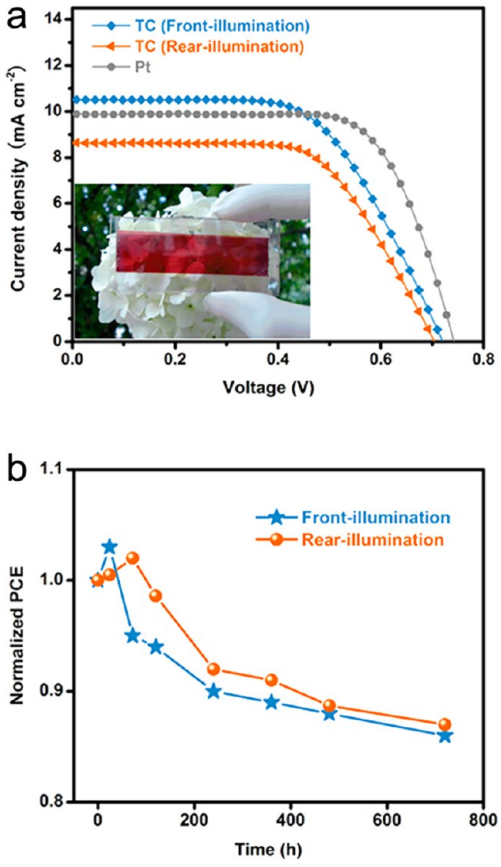

Figure 5. (a) J–V characteristics of DSCs employing transparent carbon (TC) and Pt counter electrodes (based on the optimal conditions) measured under 75 mW cm^{-2}, AM 1.5 simulated irradiation. The active area is 0.24 cm^2. The inset is a digital photograph of the large-area bifacially active transparent DSC fabricated in this work. (b) Time-course changes of the normalized power conversion efficiency (PCE) for the sealed DSC based on CE IPA/Hacac/TX-100. The device was kept under the ambient conditions, and the data were obtained under 75 mW cm^{-2}, AM 1.5 simulated irradiation with an active area of 0.24 cm^2.

Table 1. Photovoltaic Parameters of DSCs Based on Transparent Carbon CE and Pt CE Measured under 75 mW cm^{-2}, AM 1.5 Simulated Irradiation with an Active Area of 0.24 cm^2

counter electrode		V_{oc} (mV)	J_{sc} (mA cm^{-2})	FF	PCE (%)
transparent carbon (TC)	front-illumination	721	10.52	0.60	6.07
	rear-illumination	704	8.64	0.62	5.04
Pt		742	9.95	0.70	6.89

minimization of energy loss on the highly transparent carbon CE. In addition, a sealed cell (shown in the inset of Figure 5a) was employed to investigate the stability of the CE.[33] The evolution of PCE with time for sealed cell based on CE IPA/Hacac/TX-100 is shown in Figure 5b. It is found that the device maintains 86% (under front-illumination) and 87% (under rear-illumination) of initial PCE after 720 h, indicating the promising stability of this transparent carbon CE due to the good connection between the carbon film and FTO glass.

3. EXPERIMENTAL SECTION

Preparation of Transparent Carbon Electrodes. The transparent carbon electrodes were prepared through the in situ carbonization method. In a typical synthesis, 2 mL of TrionX-100 solution was dropwise added into 4 mL of isopropanol/acetylacetone solution (1:1 in volume) under stirring. A few drops of mixture solution were deposited onto a piece of well-cleaned FTO glass (7 cm × 3.5 cm) and spin-coated at 400 rpm for 5 s and 1500 rpm for 15 s. After that, the treated FTO glass was sintered at 500 °C in Ar for 30 min, resulting in the final product. The volume ratio of Triton X-100 to (isopropanol + acetylacetone) was tuned to 0.05, 0.1, 0.25, 0.5, 1.0, and 2.0, respectively, in our experiments. For comparison, the products synthesized without adding isopropanol and/or acetylacetone were also prepared using the same preparation process.

Fabrication of DSCs. To fabricate the DSCs working electrodes, the FTO glass was first immersed into a 40 mM $TiCl_4$ aqueous solution at 70 °C for 30 min; then, it was sintered at 500 °C for 30 min. After that, TiO_2 paste prepared by the hydrothermal method was doctor-bladed on as-treated FTO glass and sintered at 500 °C for 30 min; this procedure was repeated twice. Then, the TiO_2 film was treated with 40 mM $TiCl_4$ aqueous solution again as described above. For dye absorption, the as-prepared TiO_2 photoanode was immersed into a 0.5 mM dye solution in a mixture of acetonitrile and tert-butyl alcohol (volume ratio: 1:1) and kept at 60 °C for 12 h. The DSC was assembled by sandwiching the dye-absorbed TiO_2 photoanode with transparent carbon counter electrode and adding a drop of electrolyte to fill the void between the two electrodes. The electrolyte is composed of 1.0 M PMII (1-propyl-3-methyl-imidazolium iodide), 0.05 M LiI_2, 0.03 M I_2, 0.1 M GuSCN (guanidinium thiocyanate), and 0.5 M TBP (4-tert-butyl-pyridine) in a mixture of acetonitrile and propylene carbonate (PC) (volume ratio: 1:1). For the long-term stability test, the cell was sealed with Surlyn, and the electrolyte was introduced through the drilled hole on the counter electrode as reported before.[34]

Characterization. The morphology and composition of the counter electrode was studied with a scanning electron microscope equipped with an energy dispersive X-ray analyzing system (SEM/EDX, Sirion, FEG). A high solution transmission electron microscope (HRTEM, JEOL, 2010) was applied to investigate the detailed nanostructure of carbon film on the counter electrode. The sample for HRTEM was prepared as follows: the carbon film was first prepared on a copper foil by the as-mentioned method; then, the copper foil was dissolved in 0.1 mM $FeCl_3$ solution, and the carbon film was picked up by a cooper grid. UV–visible transmitted spectra of the carbon electrodes were recorded on a UV/vis spectrometer (Lambda 650S Perkin-Elmer). The Raman spectra were measured with 488 nm laser excitation by a LabRAM HR800 (the area of carbon CE was 1.5 cm^2). Electrochemical impedance spectroscopy (EIS) was performed on a CHI 660C (Shanghai China) electrochemical station in the frequency range of 0.1 Hz to 100 kHz under dark conditions. The Tafel polarization measurements were also performed on a CHI 660C (Shanghai China) electrochemical station in symmetric cells with a scan rate of 5 mV s^{-1}. The symmetric cells were made by assembling two identical carbon electrodes on each side separated by a spacer containing an electrolyte used in full function DSCs. The contact area of two carbon electrodes was controlled at 0.25 cm^2 by Scotch type. The J–V characteristics were measured under AM 1.5 irradiation (Newport 91192) with a power density of 75 mW cm^{-2}; the area of photoanodes and carbon counter electrodes were both 2.5 cm^2, and the active area was controlled at 0.24 cm^2 by a mask.

4. CONCLUSIONS

In summary, we develop a facile in situ carbonization process to fabricate transparent carbon CEs for bifacial DSCs. It is found that the precursor will dramatically affect the optical and electrochemical properties of the final product. By adjusting the composition and the concentration of the precursor, the properties of CE have been optimized preliminarily. The

dx.doi.org/10.1021/am4017472 | ACS Appl. Mater. Interfaces 2013, 5, 7432–7438

optimized transparent carbon CE exhibits sufficient electrocatalytic activity for fast reduction of I_3^- and the excellent optical transparency for requirement of rear-illumination of bifacial DSCs. The best performing device based on optimal conditions gives a high PCE of 5.04% under rear-side illumination, which approaches 85% that of the front-illumination (6.07%). Furthermore, the problem of poor mechanical stability for traditional carbon CEs also has been solved via this in situ carbonization method. The simple preparation process, low cost, high transparency, and considerable mechanical stability highlight the potential application of this carbon CE in commercial production of low-cost and effective bifacial DSCs. Further improvement of performance for bifacial DSCs can be expected if more copolymer solution with high boiling point are employed to replace the TX-100 in the future investigation.

■ ASSOCIATED CONTENT

Supporting Information

Figures S1–S4 and Tables S1–S3, in detail: Figure S1, the SEM image of pure FTO glass; Figure S2, *J*–*V* characteristics of bifacial DSCs based on four different transparent carbon CEs; Figure S3, the relationship between the different TX-100 concentrations of CE IPA/Hacac/TX-100 and the power conversion efficiency (PCE) of bifacial DSCs, the digital photographs of CE IPA/Hacac/TX-100 derived from the precursor with different TX-100 concentrations; Figure S4, the comparison between the electrochemical properties of transparent carbon CE (CE IPA/Hacac/TX-100) and the electrochemical properties of Pt CE; Table S1, the Raman ratio (I_D/I_G) and the fitted EIS parameters of the symmetrical cells with different carbon electrodes; Table S2, photovoltaic parameters of bifacial DSCs based on different transparent carbon CEs; Table S3, photovoltaic parameters of bifacial DSCs based on CE IPA/Hacac/TX-100 derived from the precursor with different TX-100 concentrations. This information is available free of charge via the Internet at http://pubs.acs.org/.

■ AUTHOR INFORMATION

Corresponding Author

*E-mail: xzzhao@whu.edu.cn.

Notes

The authors declare no competing financial interest.

■ ACKNOWLEDGMENTS

We are grateful for financial support from the National Basic Research Program of China (2011CB933300), the National Science Fund for Talent Training in Basic Science (Grant J1210061), and National Natural Science Foundation of China (Grants 51132001, 51272184).

■ REFERENCES

(1) Grätzel, M. *Nature* **2001**, *414*, 338–344.
(2) Yella, A.; Lee, H. W.; Tsao, H. N.; Yi, C.; Chandiran, A. K.; Nazeeruddin, M. K.; Diau, E. W.; Yeh, C. Y.; Zakeeruddin, S. M.; Grätzel, M. *Science* **2011**, *334*, 629–634.
(3) Chung, I.; Lee, B.; He, J.; Chang, R. P. H.; Kanatzidis, M. G. *Nature* **2012**, *485*, 486–489.
(4) Grätzel, M. *Acc. Chem. Res.* **2009**, *42*, 1788–1798.
(5) Hagfeldt, A.; Boschloo, G.; Sun, L.; Kloo, L.; Pettersson, H. *Chem. Rev.* **2010**, *110*, 6595–6663.
(6) Kroon, J. M.; Bakker, N. J.; Smit, H. J. P.; Liska, P.; Thampi, K. R.; Wang, P.; Zakeeruddin, S. M.; Grätzel, M.; Hinsch, A.; Hore, S.; Würfel, U.; Sastrawan, R.; Durrant, J. R.; Palomares, E.; Pettersson, H.; Gruszecki, T.; Walter, J.; Skupien, K.; Tulloch, G. E. *Prog. Photovoltaics: Res. Appl.* **2007**, *15*, 1–18.
(7) Murakami, T. N.; Grätzel, M. *Inorg. Chim. Acta* **2008**, *361*, 572–580.
(8) Wu, M. X.; Ma, T. L. *ChemSusChem* **2012**, *5*, 1343–1357.
(9) Veerappan, G.; Bojan, K.; Rhee, S.-W. *ACS Appl. Mater. Interfaces* **2011**, *3*, 857–862.
(10) Murakami, T. N.; Ito, S.; Wang, Q.; Nazeeruddin, M. K.; Bessho, T.; Cesar, I.; Liska, P.; Baker, R. H.; Comte, P.; Péchy, P.; Grätzel, M. *J. Electronchem. Soc.* **2006**, *153*, A2255–A2261.
(11) Joshi, P.; Zhang, L. F.; Chen, Q. L.; Galipeau, D.; Fong, H.; Qiao, Q. *ACS Appl. Mater. Interfaces* **2010**, *2*, 3572–3577.
(12) Lee, W. J.; Ramasamy, E.; Lee, D. Y.; Song, J. S. *ACS Appl. Mater. Interfaces* **2009**, *1*, 1145–1149.
(13) Lee, K. S.; Lee, W. J.; Park, N. G.; Kim, S. O.; Park, J. H. *Chem. Commun.* **2011**, *47*, 4264–4266.
(14) Ramasamy, E.; Lee, W. J.; Lee, D. Y.; Song, J. S. *Electrochem. Commun.* **2008**, *10*, 1087–1089.
(15) Wu, M. X.; Lin, X.; Wang, T. H.; Qiu, J. S.; Ma, T. L. *Energy Environ. Sci.* **2011**, *4*, 2308–2315.
(16) Xue, Y. H.; Liu, J.; Chen, H.; Wang, R. G.; Li, D. Q.; Qu, J.; Dai, L. M. *Angew. Chem., Int. Ed.* **2012**, *51*, 12124–12127.
(17) Wang, H.; Hu, Y. H. *Energy Environ. Sci.* **2012**, *5*, 8182–8188.
(18) Tai, Q. D.; Chen, B. L.; Guo, F.; Xu, S.; Hu, H.; Sebo, B.; Zhao, X. Z. *ACS Nano* **2011**, *5*, 3795–3799.
(19) Bisquert, J. *Nat. Photonics* **2008**, *2*, 648–649.
(20) Ito, S.; Zakeeruddin, S. M.; Comte, P.; Liska, P.; Kuang, D.; Grätzel, M. *Nat. Photonics* **2008**, *2*, 693–698.
(21) Li, X.; Ku, Z. L.; Rong, Y. G.; Liu, G. H.; Liu, L. F.; Hu, M.; Wang, H.; Xu, M.; Xiang, P.; Han, H. W. *Phys. Chem. Chem. Phys.* **2012**, *14*, 14383–14390.
(22) Bu, C. H.; Tai, Q. D.; Liu, Y. M.; Guo, S. S.; Zhao, X. Z. *J. Power Sources* **2013**, *221*, 78–83.
(23) Kavan, L.; Yum, J. H.; Grätzel, M. *ACS Nano* **2011**, *5*, 165–172.
(24) Wang, G. Q.; Xing, W.; Zhuo, S. P. *J. Power Sources* **2009**, *194*, 568–573.
(25) Cai, X.; Lv, Z. B.; Wu, H. W.; Hou, S. C.; Zou, D. C. *J. Mater. Chem.* **2012**, *22*, 9639–9644.
(26) Yu, K.; Wen, Z. H.; Pu, H. H.; Lu, G. H.; Bo, Z.; Kim, H. J.; Qian, Y. Y.; Andrew, E.; Mao, S.; Chen, J. H. *J. Mater. Chem. A* **2013**, *1*, 188–193.
(27) Yi, L. X.; Liu, Y. Y.; Yang, N. L.; Tang, Z. Y.; Zhao, H. J.; Ma, G. H.; Su, Z. G.; Wang, D. *Energy Environ. Sci.* **2013**, *6*, 835–840.
(28) Hauch, A.; Georg, A. *Electrochim. Acta* **2001**, *46*, 3457–3466.
(29) Wu, M. X.; Lin, X.; Hagfeldt, A.; Ma, T. L. *Angew. Chem., Int. Ed.* **2011**, *50*, 3520–3524.
(30) Kuang, C. W.; Chen, H. W.; Lin, C. Y.; Huang, K. C.; Vittal, R.; Ho, K. C. *ACS Nano* **2012**, *6*, 7016–7025.
(31) Snaith, H. J.; Schmidt-Mende, L.; Grätzel, M. *Phys. Rev. B* **2006**, *74*, 045306.
(32) Halme, J.; Vahermaa, P.; Miettunen, K.; Lund, P. *Adv. Mater.* **2010**, *22*, E210–E234.
(33) Hu, H.; Chen, B. L.; Bu, C. H.; Tai, Q. D.; Guo, F.; Xu, S.; Xu, J. H.; Zhao, X. Z. *Electrochim. Acta* **2011**, *56*, 8463–8466.
(34) Ito, S.; Chen, P.; Comte, P.; Nazeeruddin, M. K.; Liska, P.; Péchy, P.; Grätzel, M. *Prog. Photovoltaics: Res. Appl.* **2007**, *15*, 603–612.